Characterization of Y122F R2 of *Escherichia coli* Ribonucleotide Reductase by Time-Resolved Physical Biochemical Methods and X-ray Crystallography[†,‡]

W. Tong,[§] D. Burdi,[§] P. Riggs-Gelasco,[§] S. Chen,[||] D. Edmondson,[⊥] B. H. Huynh,[||] J. Stubbe,*[,§] S. Han,[▽] A. Arvai,[▽] and J. Tainer[▽]

Departments of Chemistry and Biology, Massachusetts Institute of Technology, Cambridge, Massachusetts 02139, Departments of Biochemistry and Physics, Emory University, Atlanta, Georgia 30322-3050, and Department of Molecular Biology, Scripps Research Institute, La Jolla, California 92037-1027

Received November 25, 1997; Revised Manuscript Received February 16, 1998

ABSTRACT: Ribonucleotide reductase (RNR) from *Escherichia coli* catalyzes the conversion of ribonucleotides to deoxyribonucleotides. It is composed of two homodimeric subunits, R1 and R2. R2 contains the diferric-tyrosyl radical cofactor essential for the nucleotide reduction process. The *in vitro* mechanism of assembly of this cluster starting with apo R2 or with a diferrous form of R2 has been examined by time-resolved physical biochemical methods. An intermediate, Fe^{3+}/Fe^{4+} cluster (intermediate X), has been identified that is thought to be directly involved in the oxidation of Y122 to the tyrosyl radical (•Y122). An R2 mutant in which phenylalanine has replaced Y122 has been used to accumulate intermediate X at sufficient levels that it can be studied using a variety of spectroscopic methods. The details of the reconstitution of the apo and diferrous forms of Y122F R2 have been examined by stopped-flow UV/vis spectroscopy and by rapid freeze quench electron paramagnetic resonance, and Mössbauer spectroscopies. In addition the structure of this mutant, crystallized at pH 7.6 in the absence of mercury, at 2.46 Å resolution has been determined. These studies suggest that Y122F R2 is an appropriate model for the examination of intermediate X in the assembly process. Studies with two mutants, Y356F and double mutant Y356F and Y122F R2, are interpreted in terms of the possible role of Y356 in the putative electron transfer reaction between the R1 and R2 subunits of this RNR.

Proteins containing dinuclear non-heme iron clusters involved in reductive activation of O_2 are ubiquitous in nature. They are involved in reversible O_2 binding, hydroxylation of unactivated carbon−hydrogen bonds, oxidation of a saturated to an unsaturated hydrocarbon, and oxidation of phenols to phenoxide radicals (*1*, *2*). The detailed mechanisms of these reactions, including the structures of the reactive intermediates, is a focus of many laboratories. Understanding these catalytic details and how different ligands and their stereochemistries modulate chemical reactivity is the long-range goal of all of these studies (*3*−*20*).

Our laboratories have focused on the mechanism of formation of the diferric-cluster tyrosyl radical (•Y122)[1] cofactor essential for the nucleotide reduction process catalyzed by *Escherichia coli* ribonucleotide reductase (RNR). The kinetics of cofactor assembly starting with apo R2 or diferrous R2 and rapidly mixing with Fe^{2+} and O_2 or with O_2, respectively, have been studied by stopped-flow (SF) UV/vis spectroscopy and by rapid freeze quench (RFQ) electron paramagnetic resonance (EPR) and Mössbauer spectroscopies (*5*, *9*, *10*, *21*, *22*). These studies in conjunction with crystallographic data on diferrous and diferric R2 have led to a mechanism of the reaction shown in Figure 1(*23*, *24*, *8*, *14*). When the extra reducing equivalent required to assemble the cluster is readily available, regardless of the status of the R2 (apo vs diferrous), an intermediate X has been detected that appears to be reduced to diferric R2 concomitant with oxidation of Y122 to a •Y122. A comparison of the studies starting with apo R2 and diferrous R2 suggests that a conformational change in R2 might be rate-limiting in the case of apo R2 for the rate of formation of X. Once X is formed, however, •Y122 is produced, in both cases with a rate constant of 1 s^{-1} (*22*). Intermediate X is characterized by a broad UV/vis spectrum from 360 to 365 nm and by EPR spectroscopy at 9 GHz as a sharp isotropic singlet at $g = 2.00$. RFQ Mössbauer and ^{57}Fe ENDOR spectroscopies have recently allowed formulation of X as an Fe^{3+}/Fe^{4+} cluster and the strong exchange coupling suggests that this cluster possesses at least one μ-oxo bridge (*17*). The effort to assign a detailed structure to X has been dependent on the observation that its EPR spectrum becomes anisotropic at Q band frequencies, permitting RFQ ^{1}H, ^{2}H, ^{17}O, ^{15}N and ^{14}N electron nuclear double resonance (ENDOR)

[†] This research was supported by a grant from the National Institutes of Health to J.S. (GM29295) and B.H.H. (GM47295) and by a postdoctoral fellowship to P.R.-G. from the National Institutes of Health (GM 17963).

[‡] The atomic coordinates described in this paper have been deposited in the Brookhaven Protein Data Bank (entries 1AV8 and 2AV8).

* Corresponding author.

[§] MIT.

[||] Department of Physics, Emory University.

[⊥] Department of Biochemistry, Emory University.

[▽] Scripps Research Institute.

[1] Abbreviations: RNR, ribonucleotide reductase; SF, stopped-flow; RFQ, rapid freeze quench; •Y122, tyrosyl radical; EPR, electron paramagnetic resonance; ENDOR, electron nuclear double resonance; wt, wild-type; EXAFS, extended X-ray adsorption fine structure.

S0006-2960(97)02881-X CCC: $15.00
Published on Web 04/08/1998

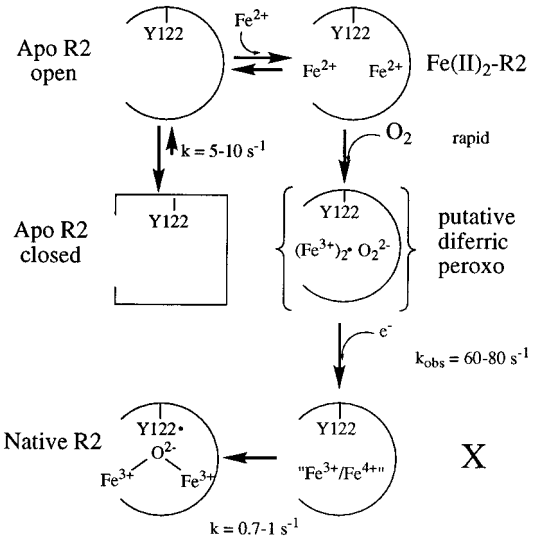

FIGURE 1: Proposed *in vitro* mechanism for the assembly of the diferric tyrosyl radical cofactor of R2.

spectroscopic analysis (*16*−*18*, *20*). To facilitate interpretation of these spectra, an R2 mutant, Y122F R2, that cannot generate a •Y122 has been very useful.

Y122F R2 was constructed initially to identify the essential tyrosyl radical of R2 (*25*). We have used this mutant as a mechanistic probe on the basis of the premise that replacement of Y122 by a nonoxidizable amino acid should result in accumulation of the iron intermediate that serves as the oxidant of Y122. The mutant functions in the expected capacity and its properties, including accumulation of a long-lived X, have facilitated the characterization of this intermediate via a number of spectroscopic methods.

Given Y122F R2's central role in characterization of X, we have investigated in detail the properties of this mutant in comparison with wt R2. In this paper we report the results of kinetic investigations of the assembly of the diferric cluster of apo Y122F R2 and diferrous Y122F R2 as examined by SF, RFQ-EPR, and Mössbauer methods. We also report the structure of this mutant at 2.46 Å resolution, crystallized at pH 7.6 in the absence of mercury. In addition we report results on the assembly of Y356F R2 and the double mutant Y122F and Y356F R2 in an effort to further probe the consequences of removal of the Y122. A role of the conserved Y356 residue is discussed.

MATERIALS AND METHODS

Natural abundance (^{56}Fe) iron wire was purchased from Baker (Phillipsburg, NJ). ^{57}Fe was purchased from Advanced Materials and Technology (New York, NY). Ferrozine and Fe atomic absorption standards were purchased from Sigma (St. Louis, MO). 2-Methylbutane (reagent grade) was purchased from Aldrich (Milwaukee, WI). Preparation of *E. coli* apo wt R2 and apo Y122F R2 was carried out as previously described (*10*). R1 was isolated from the overproducing strain C600/pMB1 (ϵ_{280nm} = 189 000 M^{-1} cm^{-1}; specific activity 1500 nmol mg^{-1} min^{-1}) (*26*). *E. coli* thioredoxin (TR) (specific activity 50 unit/mg) and thioredoxin reductase (TRR) (specific activity 800 unit/mg) were isolated from overproducing strains SK2981 (*27*) and K91/pMR14 (*28*). Oligonucleotide primers were made at the MIT Biopolymers Laboratory. The $^{56}Fe^{2+}$ and $^{57}Fe^{2+}$ stock solutions (*29*−*31*) for the Mössbauer experiments were prepared as previously described (*21*).

SDS−PAGE was carried out as described by Laemmli (*32*). R2 activity was assayed by following NADPH oxidation spectrophotometrically in a final volume of 400 μL containing 50 mM HEPES buffer (pH 7.6), 15 mM $MgSO_4$, 1 mM EDTA, 1.6 mM ATP, 1 mM CDP, 0.16 mM NADPH, 0.02 mM TR, 0.5 μM TRR, 2 μM R1, and 0.2 μM R2 (*31*). The effects of mutant Y356F R2 and the double mutant Y356F and Y122F R2 were also determined by this method.

Mathematical modeling was performed by using HopKIMSIM, a Macintosh version of Barshop and Freiden's kinetic simulation program, KINSIM (*33*). Nonlinear regression analysis on the EPR and Mössbauer kinetic data was carried out with the Git and Gear programs of Dr. R. J. McKinney and Dr. F. J. Wiegart, Central Research and Development Department, E. I. du Pont de Nemours and Co.

Preparation of R2 Mutants. The R2 Y356F and R2 Y356/Y122F mutants were constructed by the polymerase chain reaction method using standard procedures (*34*, *35*). DNA sequencing of the mutants was carried out using the dideoxy chain-termination method (*36*).

All mutants were cloned into pT7-5 and transformed into *E. coli* K38 containing pGP1-2. The mutant proteins were isolated as previously described (*10*, *37*) and the protein purity was judged by SDS−polyacrylamide gel electrophoresis. The concentrations of the apo mutant proteins were determined by absorbance at 280 nm (assuming ϵ_{280} = 120.5 mM^{-1} cm^{-1}).

Time Course of the Reaction of Apo R2 with O_2 and Fe^{2+} As Monitored by SF Absorption, RFQ-EPR, and RFQ Mössbauer Spectroscopies. SF and RFQ experiments were carried out at two different Fe^{2+}/R2 ratios as described previously (*10*, *21*, *11*). In the limiting Fe experiments, the Fe^{2+}/R2 ratio is 2.2−2.4, and in the excess Fe experiments, the Fe^{2+}/R2 ratio is 5. SF experiments were carried out on an Applied Photophysics (Leatherhead, U.K.) DX.17MV sequential SF spectrofluorometer. The reaction of apo R2 with Fe^{2+} and O_2 was initiated by mixing at 5 °C equal volumes of a solution containing 100−600 μM apo R2 in 100 mM HEPES (pH 7.7) and a solution of Fe^{2+} in 5 mM H_2SO_4, and the reaction was monitored at wavelengths between 320 and 560 nm. Both the protein solution and the Fe^{2+} solution were saturated with 1 atm of O_2.

In the RFQ-EPR and RFQ-Mössbauer experiments, 600 μM apo R2 in O_2-saturated 100 mM HEPES (pH 7.7) was mixed at 5 ± 1 °C with 1.38 mM (limiting Fe) or 3.0 mM Fe^{2+} (excess Fe) in O_2-saturated 5 mM H_2SO_4. The reaction mixture was freeze−quenched at various reaction times as described previously (*38*, *39*, *11*). EPR spectra were acquired on a Brüker ER 200D-SRC spectrometer equipped with an Oxford Instruments ESP 910 continuous-flow cryostat or on a Brüker Model ESP 300 equipped with an Oxford Instrument ESP 900 continuous-flow cryostat. Mössbauer spectra were recorded on a weak-field Mössbauer spectrometer equipped with a Janis 8DT variable-temperature cryostat and operated in a constant acceleration mode in a transmission geometry. The zero velocity of the Mössbauer spectra refers to the centroid of the room-temperature spectrum of a metallic iron foil. All Mössbauer spectra were acquired at

4.2 K with a magnetic field of 50 mT applied parallel to the γ-beam. Analysis of the Mössbauer spectra of the freeze−quenched samples to determine the quantities of the intermediate X, diferric cluster, and other iron-containing species in the reaction was carried out as previously described (*10*).

Time Course of the Reaction of Diferrous R2 with O_2 As Monitored by SF Absorption and RFQ-EPR Methods. An anaerobic solution (292 μL) of $FeSO_4 \cdot 7H_2O$ (15.4 mM) in 5 mM H_2SO_4 was mixed with an anaerobic solution of HEPES buffer (pH 7.6) (958 μL) inside a glove box. The resulting mixture was combined with apo Y122F R2 (720 μM, 1.25 mL) to give a final solution (2.5 mL) that was 360 μM in Y122F R2 and 1.8 mM in Fe^{2+}. For EPR experiments one drive syringe of the ram unit was loaded with this solution. The other drive syringe was loaded with O_2-saturated HEPES (pH 7.6). The reaction was initiated by rapid mixing and analyzed as previously described (*38*, *39*, *11*).

For SF experiments, the instument was prepared by soaking the drive syringes and the cooling bath overnight in 100 mM sodium dithionite. Just prior to loading, the drive syringes were rinsed with deoxygenated buffer. One drive syringe was filled with 590 μM Y122F R2 and 2.95 mM Fe^{2+}. The second syringe was loaded with O_2-saturated HEPES buffer. Equal volumes were mixed and the reaction was monitored at various wavelengths.

Cross-Linking Experiments under Limiting or Excess Iron Conditions. R2, Y122F R2, Y356F R2, or double mutant Y122F and Y356F R2 (600 μM) was mixed with an oxygenated solution of Fe^{2+} (1.4 or 2.95 mM, limiting or excess conditions). Alternatively, anaerobic diferrous R2 was mixed with oxygenated buffer. After the mixture was allowed to stand for 2 min, 40 μg of protein was removed and analyzed by SDS−PAGE.

Crystallization and Data Collection. Hexagonal Y122F R2 crystals of space group *P*61 (cell dimensions of $a = b =$ 136.5 Å, $c = 109.6$ Å, two subunits/asymmetric unit, $V_M =$ 3.5, solvent content = 65%) were grown from drops containing 10 mg/mL Y122F R2, 50 mM Tris, pH 7.6, and 5% glycerol by vapor diffusion against a reservoir containing 80% saturated NaCl. As a control, hexagonal crystals (cell dimensions of $a = b = 139.7$ Å, $c = 110.6$ Å, two subunits/asymmetric unit) of wt R2 crystals were obtained under the same conditions by vapor diffusion. The crystals of both wt and Y122F R2 were flash-frozen using 30% glycerol as a cryoprotectant. All wt and Y122F R2 diffraction data were collected at the Stanford Synchrotron Radiation Laboratory (SSRL), beam line 7-1 (1.08 Å radiation) at −170 °C and processed with the program packages DENZO-SCALEPACK (*40*).

The data set for wt R2 is 99% complete to 2.8 Å resolution with a R_{sym} value on all data of 8.9% and is 92% complete in the last shell between 2.92 and 2.8 Å. Diffraction data for Y122F R2 is 95% complete to 2.46 Å resolution with a R_{sym} value on all data of 5.6% and is 83% complete in the last shell between 2.55 and 2.46 Å.

Structure Determination and Refinement. The solution of the structure of both wt and Y122F R2 was obtained using molecular replacement and the wt R2 model from *E. coli* (*24*). Two rotation and translation solutions were found, corresponding to a dimer in the asymmetric unit, with AmoRe (*41*) and gave correlation coefficient = 0.74, $R =$ 34.9% for the wt structure and correlation coefficient = 0.79, $R = 30.7\%$ for the Y122F mutant structure.

For refinement, all the active-site atoms including diiron, water ligands, and μ-oxo bridge were removed from the starting model. Powell minimization of *x*, *y*, *z* and conjugation gradient refinement of individual isotropic *B*-factors were done with X-PLOR (*42*). The significance of the refinement was monitored by cross-validation with the free *R* factor (*43*), which was calculated from 6% of the data omitted from the refinement.

The metal center was modeled in the final stage of refinement to avoid model bias. The iron−ligand distance was restrained with a weak energy constant of ∼10 kcal·mol^{-1} Å^2 and target distance of 2.2 Å (*8*). The final wt model contains 2 × 340 residues, 4 ferric ions, 137 water molecules, and 2 μ-oxo bridge atoms and was refined to $R_{work} = 13.9\%$ for the data between 7.0 and 2.8 Å resolution with $|F|/\sigma \geq 1.0$. The refined Y122F R2 model, which contains 2 × 340 residues, 5 ferric ions including an extra metal (possibly iron) binding site in dimer−dimer contact, 2 μ-oxo bridge atoms, and 204 water molecules, was refined to $R_{work} = 18.1\%$ (data between 7.0 and 2.46 Å resolution with $|F|/\sigma \geq 1.0$). There is excellent agreement of bond lengths and angles with expected values for both wt and Y122F mutant model. The atomic coordinates have been deposited in the Brookhaven Protein Data Bank (entries 1AV8 and 2AV8).

RESULTS

Reaction of Apo Y122F R2 with Excess Fe^{2+} and O_2 Monitored by SF Absorption Spectroscopy. As previously described (*5*), the reconstitution of Y122F R2 was initially investigated in an effort to increase the amount of the diiron intermediate, X, involved in oxidation of Y122 to •Y122, to facilitate its spectroscopic characterization. When apo Y122F R2 is mixed with excess Fe^{2+} ($5Fe^{2+}$/R2) at 5 °C, a broad visible absorption band at 360−365 nm, characteristic of X, develops (Figure 1A, Supporting Information). In the 0.46 s spectrum, ∼40% of the final absorbance at 360 nm has developed, while the 325 nm shoulder indicative of the diferric cluster is still undetectable, suggesting that X accumulates prior to formation of the product cluster. With increasing reaction time, the spectrum of the diferric cluster develops as judged by the appearance of the more intense 360 and 325 nm features.

Scheme 1

$$\text{apo R2} \xrightarrow{k_1} \text{X} \xrightarrow{k_2} \text{diferric cluster}$$

In an attempt to estimate the rate constants for formation and decay of X, the A_{365}-versus-time traces (Figure 1B, Supporting Information) were analyzed according to the kinetic model shown in Scheme 1, giving rate constants of 2.7 s^{-1} and 0.16 s^{-1}. In contrast to expectations, formation of X in Y122F R2 is slowed relative to its formation in wt R2 by a factor of 2. In fact, the kinetic fits to the data are better than anticipated, given the simplicity of Scheme 1 and the multiple pathways by which X is reduced because of the propinquity of oxidizable amino acid residues.

Reaction of Apo Y122F R2 with Excess Fe^{2+} and O_2 Monitored by RFQ-Mössbauer Spectroscopy at 4 °C. To establish that the features associated with the SF data could

Table 1: Quantitation of **X**, Diferric Cluster, and the Putative Fast-Relaxing Ferric Species in the Reaction of Apo Y122F R2 with Excess Fe^{2+} at 5 °C in Comparison with the Same Reaction with wt R2

	Y122F R2			wt R2		
reaction time (s)	equiv of fast-relaxing Fe^{3+}	equiv of X	equiv of diferric cluster	equiv of fast -relaxing Fe^{3+}	equiv of X	equiv of diferric cluster
0.077	0.08 ± 0.05	0.4 ± 0.1	0	0.25 ± 0.06	0.53 ± 0.11	0
0.18	0.20 ± 0.05	0.65 ± 0.1	0	0.45 ± 0.06	0.84 ± 0.10	0.08 ± 0.03
0.24	0.25 ± 0.05	0.73 ± 0.1	0.05 ± 0.03	0.50 ± 0.06	0.88 ± 0.07	0.15 ± 0.04
0.32	0.3 ± 0.08	0.83 ± 0.05	0.1 ± 0.05	0.60 ± 0.11	0.98 ± 0.09	0.24 ± 0.05
0.46	0.45 ± 0.1	0.95 ± 0.05	0.14 ± 0.04	0.60 ± 0.06	0.83 ± 0.07	0.35 ± 0.06
0.63	0.5 ± 0.1	1.02 ± 0.05	0.23 ± 0.03	0.65 ± 0.06	0.68 ± 0.09	0.50 ± 0.05
1.0	0.5 ± 0.1	0.98 ± 0.05	0.33 ± 0.03	0.70 ± 0.06	0.55 ± 0.09	0.80 ± 0.10
5.0	0.45 ± 0.1	0.58 ± 0.05	0.85 ± 0.03	0.60 ± 0.06	<0.08	1.33 ± 0.08
10	0.4 ± 0.1	0.38 ± 0.08	1.23 ± 0.03			
60	0.4 ± 0.1	0	1.38 ± 0.08	0.50 ± 0.11	<0.04	1.38 ± 0.08

in fact be attributed to X, the assembly process was monitored, under identical conditions, by RFQ-Mössbauer spectroscopy. This method allows quantitation of all of the iron-containing species during the course of the reaction, given the availability of standards for diferrous R2, diferric R2, X, and a fast-relaxing ferric species thought in the case of wt R2 to deliver the extra reducing equivalent (*11*). In the case of the wt R2 assembly, 1.2 $Y^{\bullet}$ and 1.4−1.6 diferric clusters are formed during the reconstitution. In contrast to wt R2, two of the reducing equivalents for Y122F cofactor assembly must be supplied from an external source to generate the diferric cluster (*44*, *9*, *10*). Table 1 summarizes the quantitation of X and diferric cluster as a function of time using methods we have previously described for assembly of the cluster in wt R2 (Figure 2, Supporting Information, shows data graphically) (*21*). X is present at ∼1.0 equiv/R2 at ∼600 ms and decays slowly. After an initial lag phase the diferric cluster is formed. The ratio of diferric cluster/Y122F R2 at completion of the reaction is 1.38, in good agreement with wt R2 (*10*). Attempts to fit the appearance and disappearance of X using Scheme 1 have not been very successful, although analysis of the initial rate of formation of X gives a rate constant of 3.7 s^{-1}. Our inability to model the decay of X and formation of the diferric cluster is not surprising since, as described above, the normal mechanism of reduction has been obfuscated by the mutation of Y122. In fact the slow disappearance of X and the recent SF EPR experiments at room temperature of Sahlin et al. (*45*, *46*) suggest that X is reduced by multiple pathways via oxidation of specific aromatic amino acid residues within the active-site region. Inspection of the EPR spectrum of the reaction quenched at 60 s reveals ≈0.07 equiv/Y122F R2 of (an) EPR-active species other than the singlet associated with X (data not shown).

Despite the kinetic complexity, some insight into the mechanism of cofactor assembly can be obtained by qualitatively comparing wt and mutant R2 data. In Y122F R2, the t_{max} for X is 600 ms, while that for wt R2 is 220−300 ms. Furthermore, the decay of X in wt R2 is almost complete at 3 s, while decay of X in Y122F R2 is <50% complete at 5 s (data not shown). Thus as anticipated, X is more stable in the mutant. However, these SF studies also revealed that the *formation* of X in the mutant is also apparently slower than in wt. Initial rates of formation of X in Y122F R2 of ≈2.7−4 s^{-1} in comparison with 5−10 s^{-1} for wt R2 indicate that formation of X is slowed by approximately a factor of 2 (Table 2).

Table 2: Rate Constants for the Formation of X

	rate constant (s^{-1})	
starting R2	Y122F	wt
apo	≈3	5−10
diferrous	35	60−80

Previous Mössbauer studies of wt R2 indicated that a stable or slowly decaying fast-relaxing ferric species is produced concomitantly with X (*10*). It was proposed that this ferric species represents the product of the donation of the fourth electron by Fe^{2+} required for formation of X (Figure 1). Quantitative analysis of the amount of iron associated with this species indicates that it provides only half the required reducing equivalents. This putative fast-relaxing ferric species is also produced in the reaction of apo Y122F R2 with excess Fe^{2+}. As shown in Table 1, its measured quantity increases with time, accumulates to only ∼0.5 equiv/R2 between 0.6 and 1 s, and does not appear to decay significantly within 60 s. Consistent with the temporal differences in the kinetics of X between wt R2 and Y122F R2, formation of the fast-relaxing ferric species also appears to be ∼2-fold slower in Y122F R2 than in wt R2. Fitting the quantities of this species as a function of time to the equation for a first-order process gives a rate constant of 3.6 s^{-1}, which is in reasonable agreement with the rate of formation of X. These observations suggest that the fast-relaxing Fe^{3+} species is produced in a kinetically competent fashion when a Fe^{2+} donates an electron to generate X, in a manner previously proposed for wt R2. These results are surprising, for as described above, an additional reducing equivalent is required to assemble the diferric cluster of this mutant, given the unavailability of an electron from Y122. Our inability to account for the required reducing equivalents for assembly, in both wt and mutant systems, suggests that, *in vitro*, the electron can be supplied by multiple routes. In the case of Y122F R2, it further suggests that each diferric cluster may be assembled by a different mechanism: one cluster associated with efforts to oxidize residue 122 and a second that is incapable of this oxidation. Whether X is an intermediate in both types of observed clusters remains to be established. However, in all the assembly processes, starting with apo or diferrous wt or Y122F R2 that we have examined thus far, we have never seen more than 1.2 equiv of X/R2. In the case of wt R2 this number is equivalent to the amount of tyrosyl radical observed. The remaining 0.2−0.4 diferric cluster observed must arise, at a minimum, from

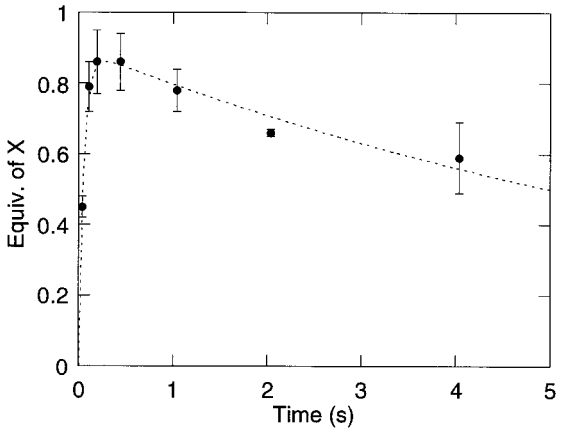

FIGURE 2: Diferrous R2 is rapidly mixed with O_2 and monitored for X by RFQ EPR spectroscopy. Each data point is the average of three experiments.

a different kinetic scheme and perhaps by a different chemical scheme as well. This observation also adds to the kinetic complexity.

Reaction of Fe^{2+}−Y122F R2 with O_2 As Monitored by SF Absorption and RFQ-EPR Spectroscopies. Recent assembly studies starting with anaerobic diferrous wt R2 have revealed that allowing Fe^{2+} binding to R2 prior to the assembly process increases the rate constant for formation of X to 60−80 s^{-1} (*19*). The rate constant for disappearance of X and formation of •Y122 (≈1 s^{-1}) is not affected. When Fe^{2+}−Y122F R2 (5 Fe^{2+}/R2) is mixed at 5 °C with O_2, the broad absorption feature at 360−365 nm, characteristic of X, rapidly accumulates before formation of the diferric cluster (data not shown).

The best fit (Figure 3, Supporting Information) to the A_{365} vs time trace from 5 to 200 ms, the time frame in which the maximum amount of X is generated as determined by EPR spectroscopy, was achieved with an equation describing two exponentials. In this time frame, rate constants of 35 ± 10 s^{-1} and 4.8 ± 1.0 s^{-1} were obtained. Both rate constants may be associated with formation of X.

The rate of formation and decay of X can also be examined starting with diferrous Y122F R2 using rapid freeze quenching and analysis by EPR spectroscopy. The results are shown in Figure 2. The data can be fit to two exponentials over the 5 ms−5 s time frame (Scheme 1), giving rate constants of 18 s^{-1} and 0.1 s^{-1}. However, the minimal set of data points between 5 and 200 ms, makes it impossible to assess the kinetic complexity within that time frame, making a direct comparson with the SF data difficult.

Comparison of rates of formation of X from apo Y122F R2 and diferrous Y122F R2 and how these differ relative to identical experiments with wt R2 is informative. X is formed in all cases, as shown by UV/vis, EPR, and Mössbauer spectroscopic analysis. On the basis of these criteria, therefore, X generated using the mutant should be an excellent tool for spectroscopic analysis. While it is not surprising that X is more stable in mutant R2, it is surprising that the rate of formation of X is decreased by a factor of ≈2−3 in the case of both apo and diferrous R2 reconstitution experiments. The hydroxyl group of Y122 affects not only the conformation of the apoprotein, as reflected in differences in apo R2 assembly experiments, but also a second step prior to generation of X (Figure 1) as reflected in diferrous reconstitution experiments. In addition, the kinetic complexity of the formation of X suggests that, as in the case of wt R2, some fraction of the diferric cluster could arise by a different pathway that may or may not involve X.

Structure of Y122F R2 at 2.46 Å Resolution at pH 7.6. The flexibility of the diiron center of R2 is the key to its catalysis. It is readily apparent that additional high-resolution structures are required to complement the existing structures (*14*) and to think about the detailed mechanism, involving ligand reorganization in the conversion of apo to the diferrous and to the diferric state of R2. Toward this end, both the wt and Y122F R2 were crystallized at pH 7.6, without Hg modification. Due to the low resolution of the newly determined wt structure at pH 7.6 and its close resemblance to the published 2.2 Å resolution structure (*8*), the focus herein will be to compare the Y122F R2 structure with the previously determined wt structure at pH 6.0 and with Hg modification. The overall structure of Y122F R2 is very similar to that of wt R2, and the rms difference between the two structures for all Cα atoms is 0.69 Å. When the two structures are superimposed and compared, each protomer in Y122F R2 is slightly contracted along an axis perpendicular to a molecular 2-fold axis of the dimer. There are significant differences in main-chain conformation for amino acid residues 51−71, 131−133, 219−224, and 286−305, which cluster near the dimer−dimer contacts in the crystal lattice. The average rms difference between Y122F R2 and wt R2 in Cα atoms of these residues is 1.1 Å and probably results from different crystal packing due to the different crystallization conditions. An extra metal binding site is found in the dimer−dimer contact region, which is discussed subsequently (Figure 4, Supporting Information).

Despite the different crystallization conditions and pH, the coordination of the diiron cofactor is close to the previously reported structure of wt *E. coli* R2 within the limits of resolution. The electron density at the diiron center in both the A and B subunits is similar and well-defined except for one water ligand and the μ-oxo bridge. The positions of two iron atoms (Fe1 and Fe2) were confirmed by a Biojvoet anomalous difference map (Figure 3). The distance between the two iron atoms is 3.4 Å for subunit A and 3.5 Å for subunit B. One ordered water molecule (Wat1201) is strongly bound to Fe2 with a 2.5 Å distance and a temperature factor of 33 $Å^2$. However, the electron density of a water ligand (Wat1202) for Fe1 and the μ-oxo bridge is weak and difficult to interpret. The peak heights of the water ligand (Wat1202) and μ-oxo bridge in the ($F_o - F_c$) map are only 2.7 and 2.5 times the rms deviation, whereas the water ligand for Fe2 is 4.7 times rms deviation (Figure 3). The positions of Wat1202 and the μ-oxo bridge are difficult to refine because these ligands are adjacent to the two high peaks in the electron density map from the ferric ions and because of the limited resolution of the data.

The positions of all the protein ligands relative to the Fe atoms are well-maintained in the Y122F R2 structure. No major conformational changes are seen in the side chains of F122 and D84. In fact, the aromatic ring of F122 has a similar orientation to that of Y122 in wt R2 (data not shown). D84, which hydrogen-bonds to Y122 in metR2, has the same bidentate coordination to the Fe1. However, the χ2 angle of D84 is changed by 30° toward F122 in subunit A. As a result, the distance of Fe1−Oδ1 (2.5 Å for subunit A and

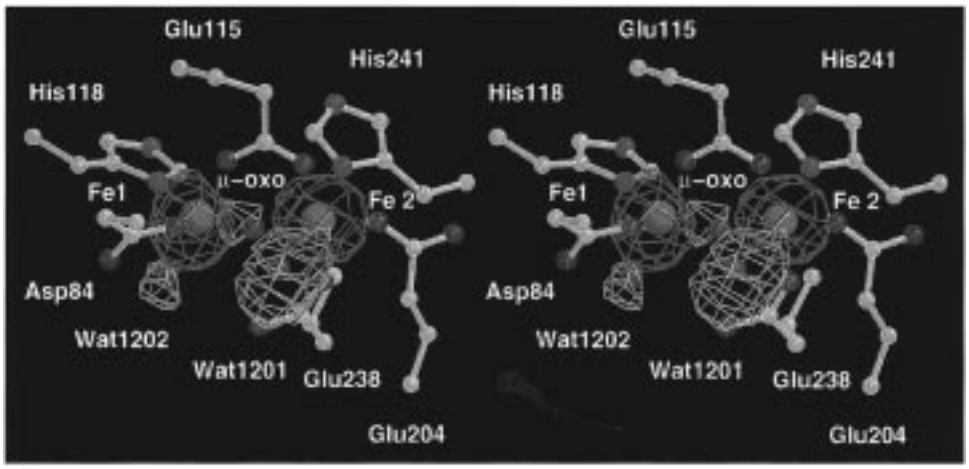

FIGURE 3: Stereoview of diiron binding site. The two Fe atoms are shown as large magenta spheres. Blue density is a Bijvoet anomalous difference map contoured at 6 σ. Light green density (2 σ) is from an $F_o - F_c$ map calculated just before the water ligands and a μ-oxo bridge are added to the model.

2.6 Å for subunit B in wt R2) and Fe1−Oδ2 of D84 (2.2 Å for subunit A and 2.5 Å for subunit B in wt R2) become 2.1 and 3.0 Å, respectively. This structural change in subunit A is consistent with the omit-refine maps obtained by omitting all the atoms within 6 Å of D84 (*47*).

An interesting structural feature in Y122F R2 is that an additional metal binding site has been found in the dimer−dimer contact region of the crystal lattice (Figure 4, Supporting Information). The corresponding site in the wt metR2 is vacant and solvent-exposed. The metal has a similar maximum density in an anomalous difference map to that of the diiron cofactor, indicating full occupancy. Since Y122F R2 was purified under identical conditions to the wt R2, by addition of iron and ascorbate to the crude *E. coli* cell extracts prior to the purification, this third metal, possibly iron, unique to the mutant R2 may be of chemical interest. Not suprisingly, the binding site for this monomeric metal is different from the cysteine residues that form Hg binding sites in the published wt metR2 structure (*8*). Five ligands bind to this metal atom and include the side chains of two residues, Glu69 from both the A and B subunits of two different dimers, and three water molecules. The geometry of this metal is close to a trigonal bipyramid with three water molecules as equatorial ligands and two Glu69 residues as axial ligands (Figure 5, Supporting Information, presents the difference density for the third metal and its water ligands). All three water ligands are stabilized by forming hydrogen bonds to nearby amino acid residues His68, Glu69, Arg221, and the backbone of Ile 297 of both subunits A and B. An important conclusion from this structure is that the pH of 6 and the presence of ethyl Hg required to obtain the first structures of R2 have not altered the ligand organization under more physiological condtions.

Reaction of Apo R2 with Limiting Fe^{2+} Is Accompanied by R2 Cross-Linking: *A Role for Y_{356}*? Our previous studies revealed that when apo Y122F R2 is mixed with limiting iron (2.3 Fe^{2+}/R2) and the required reducing equivalent is not readily available, the assembly of the iron-cluster tyrosyl cofactor is accompanied by a transient absorption change at 410 nm (*4*, *9*). We suggested at that time that since F122 could not be oxidized, the reducing equivalents were provided, at least in part, by an oxidation of a second tyrosine. The conservation of Y356 among all R2s and its importance in the nucleotide reduction process revealed by mutagenesis studies (*48*) suggested that it might be a viable candidate for this transient species. If the transient is in fact associated with a Y•, using an extinction coefficient identical to that for •Y122 suggested that at a maximum, 10% of the protein is in this form. Y356 is located in the C-terminal tail of R2, a portion of the protein not observable crystallographically in the original structures or in the present structures, due to thermal lability.

There are now several examples in the literature of observed cross-linking of subunits of enzymes that have been mutated such that a chemically reactive intermediate will have an enhanced lifetime. In the absence of the natural reductant, amino acid residues with oxidizable side chains can be oxidized and the information could potentially be transferred to the surface of the protein where chemistry with a second protein molecule may be observed. Tew and Ortiz de Montellano (*49*) have demonstrated the formation of intramolecular dityrosine cross-linkages in the reaction of metmyglobin with peroxide. A similar mechanism involving surface Y• has been proposed to account for the cross-linking of cytochrome *c* peroxidase, which occurs when the ferrous enzyme reacts with O_2 in the absence of substrates (*50*). To determine whether the formation of the putative transient radical species in the limiting Fe^{2+} reaction also causes an intermolecular cross-linking reaction, the products of the limiting Fe^{2+} reactions were analyzed by SDS−PAGE. As shown in Figure 4, only one major band is observed in each of the reactions involving excess Fe^{2+}(Figure 4, lanes 3 and 4). These bands have migratory properties identical to that of native R2, 43.7 kDa. However, when a concentrated sample (1 mM of apo YI22F R2 or apo wt R2) reacts with limiting Fe^{2+}, the SDS−polyacrylamide gel of the reaction mixtures shows that part of the R2 present is converted to a band corresponding to a dimeric form. These results indicate that protein−protein cross-linking can occur under these conditions.

Characterization of Y356F R2 and Y122F and Y356F R2. If the cross-linking results and the observation of the transient absorption at 410 nm are indicative of formation of a transient Y356•, its mutation to a phenylalanine should preclude both observations. We initially prepared and characterized Y356F R2. This protein has a UV/vis spectrum

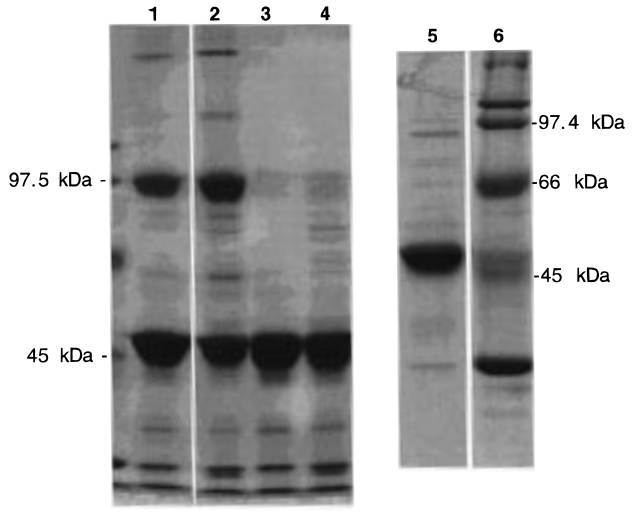

FIGURE 4: SDS−PAGE of the assembly of apo R2, apo Y122F R2, and apo Y122F and Y356F R2 and monitoring by SDS−PAGE for protein cross-linking. Conditions are as follows: lane 1, apo R2 and 2.3 Fe^{2+}/R2; lane 2, apo Y122F R2 and 2.3 Fe^{2+}/R2; lane 3, apo R2 with 5 Fe^{2+}/R2; lane 4, apo Y122F R2 and 5 Fe^{2+}/R2; lane 5, apo Y356F and Y122F R2 and 2.3 Fe^{2+}/mutant R2; lane 6, molecular weight standards. The spaces in between the lanes indicate that different gels were run.

indicative of a diferric-tyrosyl radical cofactor and contains 2.8 Fe/R2 and 1.1 $Y^{\bullet}$/R2. Reaction of apo Y356F R2 with 5Fe^{2+} and O_2 results in formation of $^{\bullet}$Y122 with a rate constant of 0.7 s^{-1}. Thus the properties of this single mutant are very similar to those of wt R2.

The double mutant Y122F and Y356F R2 was thus prepared. Its visible spectrum is very similar to that of Y122F R2 and contains 2.8 irons. Both mutant R2s have activity for nucleotide reduction ~0.5% that of wt R2. This is the estimated amount of contaminating wt R2 thought to be present in all preparations due to expression in *E. coli* and our inability to delete the wt gene due to lethality. These results, those of Climent et al. (*51*, *48*) with Y356A R2, and the conservation of Y356 suggest that it plays an important function in the reduction process. However, it does not appear to play a role in the assembly of the cofactor.

To address the question of whether Y356 gives rise to the transient absorption feature at 410 nm observed in the limiting Fe^{2+} Y122F R2 reconstitution experiment, the reconstitution of apo Y122F and Y356F R2 with limiting iron was examined. Even at 205 μM protein (this is 10 times the concentration of protein used in the corresponding Y122F R2 experiments), no transient feature was detected. Furthermore, a similar reconstitution experiment carried out with 1 mM mutant failed to reveal any cross-linked dimer R2 (Figure 4, lane 5). Thus, both pieces of data support the proposal that the transient 410 nm visible feature may be associated with Y356 on the surface of R2.

The reconstitution of apo Y356F and Y122F R2 was also examined with an excess of Fe^{2+} (5Fe^{2+}/R2). The intermediate X, an Fe^{4+}/Fe^{3+} species, is detected (data not shown), but its decay is much slower than X observed with either wt or Y122F R2. At 4 s, 0.7 equiv of X/R2 are still present. This property will be useful in examining X spectroscopically in the absence of liquid isopentane used in freeze−quenching experiments.

DISCUSSION

Y122F R2 has been used to study intermediate X, proposed to be the direct precursor to the diferric tyrosyl radical cofactor of wt R2 essential for nucleotide reduction. This mutation was chosen to increase the lifetime of X, as F is more difficult to oxidize than Y, and to eliminate the EPR signal associated with the $Y^{\bullet}$ to facilitate interpretation of RFQ ENDOR experiments (*16*−*18*, *20*). This mutant has now been used for spectroscopic characterization of X by RFQ ENDOR and EXAFS (*52*) and hand-quenched resonance Raman. Thus the relationship between its diferric cluster assembly relative to wt R2 is important to establish.

We have therefore examined the assembly process from apo Y122F R2 and diferrous Y122F R2, following the progress of the reaction by SF UV/vis spectroscopy and RFQ EPR and Mössbauer methods. Using these methods, X has been identified and is spectroscopically indistinguishable from X generated with wt R2. The kinetics of formation and disappearance of X are much more complex than with wt R2. Recall that, in the assembly of active diferric-tyrosyl radical cofactor of R2, an extra reducing equivalent is essential for the $4e^-$ reduction of O_2 to H_2O (*53*, *44*, *10*). Additional complexity arises in the case of wt R2, in that only 1.2 $Y^{\bullet}$ are observed/1.4−1.6 diferric clusters. Thus despite the observation of fully occupied iron sites in the original crystal structure at pH 6 and the present structure at pH 7.6, biochemical analysis never reveals a full complement of iron for reasons that are not understood. In the case of Y122F R2, further complexity results from the requirement of two extra electrons to generate the diferric clusters, rather than the one electron for wt R2 assembly (*44*).

How could replacement of a single hydroxyl with a hydrogen (Y to F) affect the rate of formation of X? The working model (Figure 1) for this process is proposed to require reductive cleavage of the O−O bond derived from O_2 (*22*, *19*, *54*), presumably in the diferric peroxide state. This process may involve protonation of one of these oxygens to generate X, the Fe^{3+}/Fe^{4+} cluster with a μ-oxo bridge and a H_2O or a disordered hydroxide attached to the Fe^{3+} (*55*). The hydroxyl proton of Y122 could be a source of the proton assisting in O−O bond cleavage, with one of the oxygens from O_2 ultimately resulting in water or disordered hydroxide ligand formation. Deprotonation of Y122 would also facilitate its own oxidation, as phenolates are easier to oxidize than phenols. Thus Y122F R2, unable to assist in the protonation of an intermediate required for formation of X, would be expected to have a reduced rate of its formation.

The model in Figure 1 also requires an electron for assembly of X. Previous workers (*56*) have pointed out the presence of a putative hydrogen bond between the hydroxyl of Y122 and a carboxylate oxygen of D84, a ligand to the adjacent iron in the diferrous R2 state. In the case of Y122F R2, this interaction is absent. Could this interaction in some way facilitate the reduction of a precursor to X by altering the rate of delivery of the required reducing equivalent or could the interaction play a role in the tremendous structural reorganization that must accompany conversion of the diferrous R2, in which the two irons are 3.8 Å apart, to X, in which they are 2.49 Å apart (*52*)? The observation of 0.5 equiv of fast-relaxing ferric species in the reconstitution

both of apo wt and Y122F R2 suggests that altered electron transfer is not the case. Recent EXAFS data suggest that X in both the wt and mutant R2 possesses a short iron−iron distance, although the Y122F R2 reconstituted from apo Y122F R2 is subtly different. These data, coupled to the similarities in the mutant and wt structures of R2, suggest that the major source of kinetic complexity is thus most likely associated with the importance of the proton of the hydroxyl group of Y122 in the chemistry and the iron cluster rearrangement during assembly.

In addition to the altered rate in formation of X in Y122F R2, its rate of disappearance is also altered relative to wt R2 as expected. An examination of the crystal structure of R2 indicates a number of easily oxidizable aromatic residues (W48, W107, and W111) within 4−8 Å of the cofactor, which could potentially reduce X in the absence of its normal reductant (*45*, *46*, *57*). Oxidation of these residues has been demonstrated in recent studies using room-temperature rapid-flow EPR spectroscopy in which six species were detected (*46*). At least two of these species have been identified by deuteration experiments as derivatives of tryptophan radicals. The time scale and amounts of these radicals are slow (minutes) and small (<6%), respectively. As previously demonstrated in many heme-dependent systems, when the normal substrate is not available to be oxidized, the reactive species can be reduced by many pathways, none of which kinetically appears to be physiologically significant. Small amounts of oxidized amino acids are also consistent with the results of our cross-linking experiments (Figure 4) and our inability to model the kinetics of the formation and decay of X.

Role of Y356? Bollinger et al. (*4*) detected by SF methods during the reconstitution of Y122F R2 with limiting iron a transient species with a sharp absorption feature at 410 nm. This species was generated on the second time scale and represented, assuming it is a Y•, 0.1 equiv/equiv of R2. We originally proposed that this transient absorption feature could be associated with •Y356 and could be mechanistically interesting given that the •Y122 on R2 is proposed to generate a transient thiyl radical on 439 (*58*) of R1. Y356 has been proposed to be on the pathway (*59*).

Y356F R2, as with the previously reported Y356A R2, is inactive with respect to nucleotide reduction (*46*). However, the mutant is structurally and functionally intact with respect to the *in vitro* assembly process. We thus prepared the double mutant, Y356F and Y122F R2, and looked for disappearance of the transient 410 nm feature. No transient feature was observed. In addition, examination of the R2 mutant proteins from apo R2 reconstitution with limiting iron by SDS−PAGE revealed that R2 is observed as a dimer of protomers with Y122F R2 but not with the double mutant (Figure 4). These studies suggest that Y356 might be the source of the transient visible absorption feature and cross-linking. However, despite extensive efforts, we have thus far failed to detect a transient Y• by RFQ-EPR spectroscopy. Given the concentrations predicted by SF spectroscopy and the presence of the EPR-active X that dominates the spectum, it is possible that the signal, depending on the hypefine interaction with the β-hydrogens of Y• (*60*), could be obscured by the EPR spectrum of X. However, recent rapid-flow EPR studies (*45*) at 25 °C, which detected small amounts of a large number of oxidized aromatic residues, failed to reveal the presence of a signal that could be unambiguously associated with a Y•. In addition, we carried out a reconstitution experiment with diferrous Y122F R2 under limiting iron conditions. We thought that rapid generation of X (35 s^{-1}) would increase the amount of the transient 410 nm species, due to the intramolecular nature of the reaction. However, in contrast to expectations, none of the 410 nm feature was detected. Thus the importance of this transiently generated species is still open to question, although the cross-linking results and disappearance of the transient 410 nm feature with the mutant are intriguing.

SUPPORTING INFORMATION AVAILABLE

Five figures showing (1) the development of the absorption spectrum of the diferric cluster upon mixing apo Y122F R2 with O_2 and excess Fe^{2+}; (2) a time course of the development of intermediate X and the diferric cluster on mixing apo Y122F R2 with excess Fe^{2+} using Mössbauer spectroscopy; (3) the formation of X monitored at 365 nm upon mixing diferrous R2 with O_2; (4) the X-ray structure of Y122F R2 showing the Cα backbones of the two dimers of R2 and one of the dimer−dimer contacts in the crystal lattice; and (5) a stereo drawing of the third, new metal binding site in the dimer−dimer contact between the R2 protomers (5 pages). Ordering information is given on any current masthead page.

REFERENCES

1. Feig, A. L., and Lippard, S. J. (1994) *Chem. Rev. 94*, 759−805.
2. Wallar, B. J., and Lipscomb, J. (1996) *Chem. Rev. 96*, 2625−2658.
3. Nordlund, P., Sjöberg, B.-M., and Eklund, H. (1990) *Nature 345*, 593−598.
4. Bollinger, J. M., Jr., Edmondson, D. E., Huynh, B. H., Filley, J., Norton, J. R., and Stubbe, J. (1991) *Science 253*, 292−298.
5. Bollinger, J. M., Jr., Stubbe, J., Huynh, B. H., and Edmondson, D. E. (1991) *J. Am. Chem. Soc. 113*, 6289−6291.
6. Nordlund, P., Dalton, H., and Eklund, H. (1992) *FEBS Lett. 307*, 257−262.
7. Fox, B. G., Hendrich, M. P., Surerus, K. K., Andersson, K. K., Froland, W. A., Lipscomb, J. D., and Munck, E. (1993) *J. Am. Chem. Soc 115*, 3688−3701.
8. Nordlund, P., and Eklund, H. (1993) *J. Mol. Biol. 232*, 123−164.
9. Bollinger, J. M., Jr., Tong, W. H., Ravi, N., B. H., Edmondson, D. E., and Stubbe, J. (1994) *J. Am. Chem. Soc. 116*, 8024−8032.
10. Bollinger, J. M., Jr., Tong, W. H., Ravi, N., Huynh, B. H., Edmondson, D. E., and Stubbe, J. (1994) *J. Am. Chem. Soc. 116*, 8015−8023.
11. Bollinger, J. M., Jr., Tong, W. H., Ravi, N., Huynh, B. H., Edmondson, D. E., and Stubbe, J. (1995) *Methods Enzymol. 258*, 278−303.
12. Liu, K. E., Valentine, A. M., Qui, D., Edmondson, D. E., Appelman, E. H., Spiro, T. G., and Lippard, S. J. (1995) *J. Am. Chem. Soc. 117*, 4997−4998.
13. Liu, K. E., Valentine, A. M., Wang, D., Huynh, B. H., Edmondson, D. E., Salifoglou, A., and Lippard, S. J. (1995) *J. Am. Chem. Soc. 117*, 10174−10185.
14. Nordlund, P., and Eklund, H. (1995) *Curr. Opin. Struct. Biol. 5*, 758−766.
15. Rosenzweig, A. C., Nordlund, P., Takahara, P. M., Frederick, C. A., and Lippard, S. J. (1995) *Chem. Biol. 2*, 409−418.
16. Burdi, D., Sturgeon, B. E., Tong, W. H., Stubbe, J., and Hoffman, B. M. (1996) *J. Am. Chem. Soc. 118*, 121−134.

17. Sturgeon, B. E., Burdi, D., Chen, S., Huynh, B. H., Edmondson, D. E., Stubbe, J., and Hoffman, B. M (1996) *J. Am. Chem. Soc. 118*, 7551−7557.
18. Deleted in proof.
19. Tong, W. H., Chen, S., Lloyd, S., Edmondson, D., Huynh, B. H., and Stubbe, J. (1996) *J. Am. Chem. Soc. 118*, 2107−2108.
20. Willems, J. P., Lee, H. I., Burdi, D., Doan, P. E., Stubbe, J., and Hoffmann, B. M. (1997) *J. Am. Chem. Soc 119*, 9603−9613.
21. Ravi, N., Bollinger, J. M., Jr., Tong, W. H., Ravi, N., B. H., Edmondson, D. E., and Stubbe, J. (1994) *J. Am. Chem. Soc. 116*, 8007−8014.
22. Tong, W. (1996) Ph.D. Thesis, Massachusetts Institute of Technology, Cambridge, MA, pp 1−478.
23. Åberg, A., Nordlund, P., and Eklund, H. (1993) *Nature* (*London*) *361*, 276−8.
24. Nordlund, P., Aaberg, A., Uhlin, U., and Eklund, H. (1993) *Biochem. Soc. Trans. 21*, 735−8.
25. Larsson, A., and Sjöberg, B. M. (1986) *EMBO J. 5*, 2037−40.
26. Salowe, S. P., and Stubbe, J. (1986) *J. Bacteriol. 165*, 363−366.
27. Lunn, C. A., Kathju, S., Wallace, B. J., Kushner, S., and Pigiet, V. (1984) *J. Biol. Chem. 259*, 10469−10474.
28. Russel, M., and Model, P. (1985) *J. Bacteriol. 163*, 238−242.
29. Massey, V. (1957) *J. Biol. Chem. 229*, 763−770.
30. Stookey, L. L. (1970) *Anal. Chem. 42*, 779−781.
31. Salowe, S. P., Ator, M., and Stubbe, J. (1987) *Biochemistry 26*, 3408−3416.
32. Laemmli, U. K. (1970) *Nature 227*, 680−685.
33. Barshop, B. A., Wrenn, R. F., and Frieden, C. (1983) *Anal. Chem. 46*, 1248.
34. Ho, S. N., Hunt, H. D., Horton, R. M., Pullen, J. K., and Pease, L. R. (1989) *Gene 77*, 51−59.
35. Nelson, R. M., and Long, G. M. (1989) *Anal. Biochem. 180*, 147−150.
36. Sanger, F., Nicklen, S., and Coulson, A. R. (1977) *Proc. Natl. Acad. Sci. U.S.A. 74*, 5463−67.
37. Tabor, S., and Richardson, C. (1985) *Proc. Natl. Acad. Sci. U.S.A. 82*, 1074−1078.
38. Bray, R. C. (1961) *Biochem J. 81*, 189.
39. Ballou, D. P., and Palmer, G. (1974) *Anal. Chem. 46*, 1248.
40. Otwinowski, Z., and Minor, W. (1997) *Methods Enzymol. 276*, 307−326.
41. Navaza, J. (1994) *Acta Crystallogr. A50*, 157−163.
42. Brunger, A. T., Karplus, M., and Petsko, G. A. (1989) *Acta Crystallogr. A45*, 50−61.
43. Brunger, A. T. (1993) *Acta Crystallogr. D49*, 24−36.
44. Elgren, T. E., Lynch, J. B., Juarez, G. C., Muenck, E., Sjoberg, B. M., and Que, L., Jr. (1991) *J. Biol. Chem 266*, 19265−19268.
45. Sahlin, M., Lassmann, G., Poetsch, S., Slaby, A., Sjöberg, B. M., and Gräslund, A. (1994) *J. Biol. Chem 269*, 11699−11702.
46. Sahlin, M., Lassmann, G., Pötsch, S., Sjöberg, B. M., and Gräslund, A. (1995) *J. Biol. Chem. 270*, 12361−12372.
47. Hodel, A., Kim, S. H., Brunger, A. (1992) *Acta Crystallogr. A48*, 851.
48. Climent, I., Sjöberg, B.-M., and Huang, C. F. (1992) *Biochemistry 31*, 4801−4807.
49. Tew, D., and Ortiz de Montellano, P. R. (1988) *J. Biol. Chem. 263*, 17880−17886.
50. Miller, M. A., Bandypadhyay, D., Mauro, J. M., Traylor, T. G., and Kraut, J. (1992) *Biochemistry 31*, 2780−2797.
51. Climent, I., Sjöberg, B.-M., and Huang, C. Y. (1991) *Biochemistry 30*, 5164−5171.
52. Riggs-Gelasco, P. J., Shu, L., Chen, S., Burdi, D., Huynh, B. H., Que, L., and Stubbe, J. (1998) *J. Am. Chem. Soc. 120*, 849−860.
53. Ochiai, E., Mann, G. J., Graslund, A., and Thelander, L. (1990) *J. Biol. Chem 265*, 15758−15761.
54. Burdi, D., Riggs-Gelasco, P., Tong, W., Stubbe, J., Willems, J. P., Lee, H. I., Doan, P. E., Hoffman, B. M., Shu, L., Que, L., Chen, S., Edmondson, D., and Huynh, B. H. (1997) *Steenbock Symp. 25*, 85−95.
55. Burdi, D., Willems, J. P., Antholine, W. E., Riggs-Gelasco, P., Stubbe, J., and Hoffman, B. M. (1998) *J. Am. Chem. Soc.* (submitted for publication).
56. Logan, D. T., Su, X. D., Aberg, A., Rngnstrom, K., Hajdu, J., Eklund, H., and Nordlund, P. (1996) *Structure 15*, 1057−1066.
57. Katterle, B., Sahlin, M., Schmidt, P. P., Potsch, S., Logan, D. T., Graslund, A., and Sjoberg, B. M. (1997) *J. Biol. Chem. 272*, 10414−10421.
58. Stubbe, J. (1990) *J. Biol. Chem. 265*, 5329−5332.
59. Ekberg, M., Sahlin, M., Eriksson, M., and Sjöberg, B.-M. (1996) *J. Biol. Chem. 271*, 20655−20659.
60. Schmidt, P. P., Andersson, K. K., Barra, A.-L., Thelander, L., and Graslund, A. (1996) *J. Biol. Chem. 271*, 23615−23618.
61. Kraulis, P. J. (1991) *J. Appl. Crystallogr. 24*, 946−950.

BI9728811